

Knee Cartilage Extraction and Bone-Cartilage Interface Analysis from 3D MRI Data Sets

José G. Tamez-Peña, Monica Barbu-McInnis and Saara Totterman
VirtualScopics, 350 Linden Oaks, Rochester NY, 14625, USA

ABSTRACT

This work presents a robust methodology for the analysis of the knee joint cartilage and the knee bone-cartilage interface from fused MRI sets. The proposed approach starts by fusing a set of two 3D MR images of the knee. Although the proposed method is not pulse sequence dependent, the first sequence should be programmed to achieve good contrast between bone and cartilage. The recommended second pulse sequence is one that maximizes the contrast between cartilage and surrounding soft tissues. Once both pulse sequences are fused, the proposed bone-cartilage analysis is done in four major steps. First, an unsupervised segmentation algorithm is used to extract the femur, the tibia, and the patella. Second, a knowledge based feature extraction algorithm is used to extract the femoral, tibia and patellar cartilages. Third, a trained user corrects cartilage misclassifications done by the automated extracted cartilage. Finally, the final segmentation is revisited using an unsupervised MAP voxel relaxation algorithm. This final segmentation has the property that includes the extracted bone tissue as well as all the cartilage tissue. This is an improvement over previous approaches where only the cartilage was segmented. Furthermore, this approach yields very reproducible segmentation results in a set of scan-rescan experiments. When these segmentations were coupled with a partial volume compensated surface extraction algorithm the volume, area, thickness measurements show precisions around 2.6%.

Keywords: Cartilage extraction, Multispectral Segmentation, Cartilage-Bone Interface, Deformable Models

1. INTRODUCTION

Quantitative analysis of cartilage morphometry from magnetic resonance imaging (MRI) is becoming the standard for the assessment of osteoarthritis(OA) for progression evaluation and treatment monitoring; but care has to be taken to ensure the validity of the end-points.¹ OA modifying drugs can take advantage of the sensitivity and specificity of the new cartilage quantification techniques which report inter class correlations(ICC) above 0.98 and coefficients of variations below 4.0%^{2,3,4,5,6,7} Although these new techniques have the potential to be applied into large population studies, most of them requires highly trained users to achieve the optimal performance; therefore, limiting their applicability.¹ The requirement of highly trained users can be avoided by the development of more automated segmentation algorithms. This automatization can be achieved in the future by the use MR images with very good contrast and high spatial resolution. In the mean time the use of advanced imaging techniques like image fusion and multi-spectral segmentation are helping in the creation of complex algorithms for the analysis of the human knee cartilage. Furthermore, the progression of computer graphics has allowed the creation of powerful editing tools that simplify the interactive segmentation required by semi-automated approaches like the one presented in this work.

The use of only a single pulse sequence for cartilage segmentation limits the amount of automatization that can be achieved. Furthermore, it has been shown that a single pulse sequence is not sufficient for the accurate evaluation of the stage of OA on the knee joint^{8,9}. The best sequences that reflect the stage of structural cartilage damage are not the best for the quantification of subchondral bone,² fluid, or bone marrow edema. On the other hand, the applicability of multiple pulse sequences for cartilage segmentation has been hindered by the lack of good registration techniques that address the articulated nature of the joints. Other factor that affects the applicability of multiple pulse sequences is the chemical shift artifact that makes the registration

Further author information: (Send correspondence to J.G.T)

J.G.T.: E-mail: tamez@virtualscopics.com, Telephone:(585) 249-6231

M.B.: E-mail: monica@virtualscopics.com

S.T.: E-mail: saara_totterman@virtualscopics.com

problem more challenging.¹⁰ Although the articulated registration of multiple pulse sequences is still an issue to be accurately solved, there have been some preliminary work that show the advantage of the use of multiple pulse sequences for a multi-spectral segmentation of the knee joint^{11,12,13}. The main advantage of multi-spectral segmentation is that a fully automated process for the bone and cartilage segmentation can be developed for the normal knee.¹⁴ The disadvantage of the former method is that it has problems for the segmentation of OA knees where cartilage and subchondral bone have different signal properties than those of the normal knee. This limitation does not affect much the bone segmentation; therefore, the multi-spectral approach still is very useful in the automatization of the cartilage extraction. This multi-spectral approach is used in this work for the extraction of the bone tissue. However, it is not used for the extraction of the cartilage tissue that shows the biggest signal variations in OA subjects. Furthermore, the lack of contrast between soft tissue and certain regions of the cartilage limits the use of a fully automated approach even for multi-spectral data sets.

Cartilage inhomogeneities and minimum inter-tissue contrast are the biggest challenges for cartilage segmentation. These problems have been partially solved by deformable models approaches like snakes.¹⁵ The deformable template approach is also proposed in this paper to address the inhomogeneity of the cartilage signal and the low contrast between cartilage and adjacent tissues. However, the proposed model differs from snakes in to major ways. First, the deformable model is three dimensional(3D). Second, the 3D deformable model is automatically derived from the topology of the bones. The proposed deformable model adapts to the cartilage boundaries based on internal mesh forces and external image driven forces. Once the deformable model adapts to the external boundaries of the cartilage, the users has the freedom to correct misplaced cartilage boundaries. The final segmentation is done after the whole bone cartilage segmentation are refined by the minimization of the local a-posterior probability based on a Gibbs random field model of the labeled-image data pair.¹⁶ The final segmentation is composed of a full cartilage segmentation and all the bone tissue contained in the MRI field of view (FOV). This full joint segmentation allows the automated analysis of the bone-cartilage interface where contact areas, cartilage thickness and cartilage volumes are extracted. The next section explains in detail the proposed methodology for bone and cartilage segmentation, and the methodology used for the bone-cartilage interface quantification. The results section will report the performance of applying the proposed method to the cartilage and bone segmentation on a series of six knee MR scans of a female volunteer carried over one year period.

2. METHODS

2.1. DATA SETS

Three female volunteers were imaged on a 1.5T MR scanner. One female volunteer was scanned in five different occasions within a year: Baseline, three weeks, two months, six months, and one year. The scans used the same resolution a 256x256 matrix on a 120 cm FOV. All the scans had a routine 3D gradient recall echo (GRE) fat suppressed sequence; while three of the scans had a second T_2 weighted 3D GRE routine sequence. To test the impact of MR parameters, the echo time and the repetition time were slightly different on each scan. The TR went from 47.0 ms to 50 ms. The TE was between 3.0 and 21 ms. The change on the TR and TE made some impact in the image quality but at least all the MR showed cartilage with similar morphometry characteristics. Figure 1. shows the a single slice of the subject MR images trough time. As seen on these sample images the amount of contrast between bone and surrounding tissue was different among the scans.

2.2. Analysis

The segmentation of the cartilage is executed following the flowchart described in figure 2. The segmentation of the cartilage depends on the correct choice of the first pulse sequence. This sequence has to be one that shows the cartilage tissue as a hype-intense tissue compared to the signal properties of the surrounding tissues. The second pulse sequence is chose in such a way that the combination of both shows the best contrast between bone and fat, and between cartilage and fluid. This contrast combination is usually achieved by the routine fat suppressed T1 weighed scan and by a routine 3D GRE T2 weighed scan, like the ones done similar to the images acquired on our scanned volunteer. The segmentation of the image started by first combining the two pulse sequences into a single multi-spectral data set. The combination of the two pulse sequence was achieved by first doing the registration of the second pulse sequence to the first pulse sequence. Although knee flexion has to be

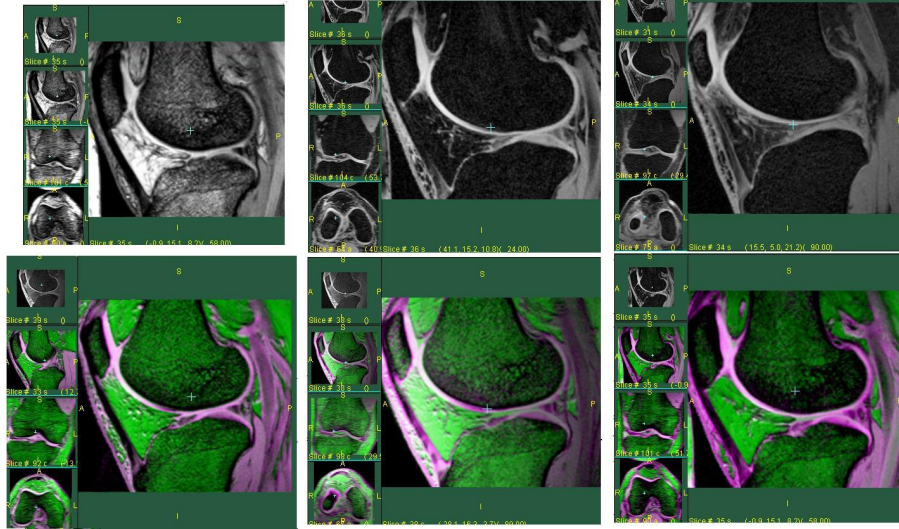


Figure 1. Middle Slice trough the five different analyzed scans. Top left, a T_2 weighted MRI of the knee. Top center, the first fat suppressed scan. Top right, the second fat suppressed scan. From Bottom left to bottom right, a slice trough the fused data sets

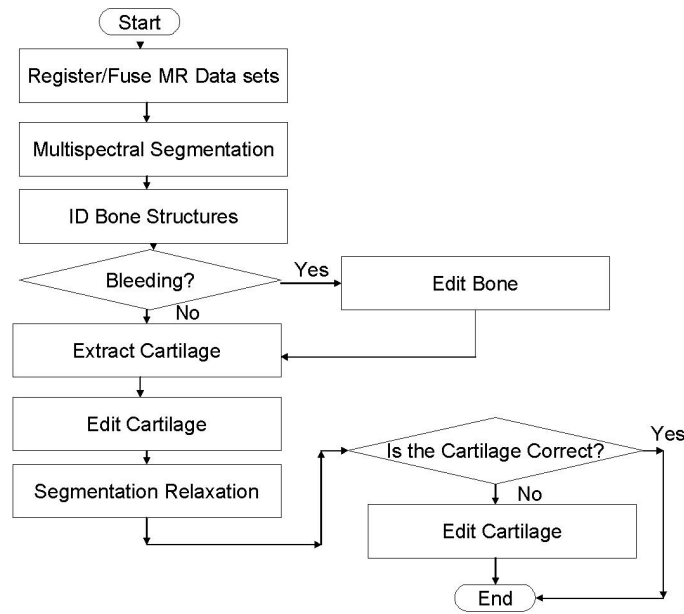


Figure 2. Bone-Cartilage Segmentation Flow Chart

taken into account, at this time we assumed that the subject didn't flex the knee or tighten her muscles between scans. Therefore, the registration was assumed rigid was done by a normalized mutual information approach.¹⁷ Once the images are registered both are stored in a dual-band multi-spectral structure.

2.2.1. Bone Segmentation

The multi-spectral image then was segmented using a the segmentation algorithm suggested by Tamez¹²; but on the decimated space. The decimation is accomplished by sampling every other voxel in the acquired slice. Once the data has been sub-sampled this is segmented and the segmentation result is extrapolated to the original

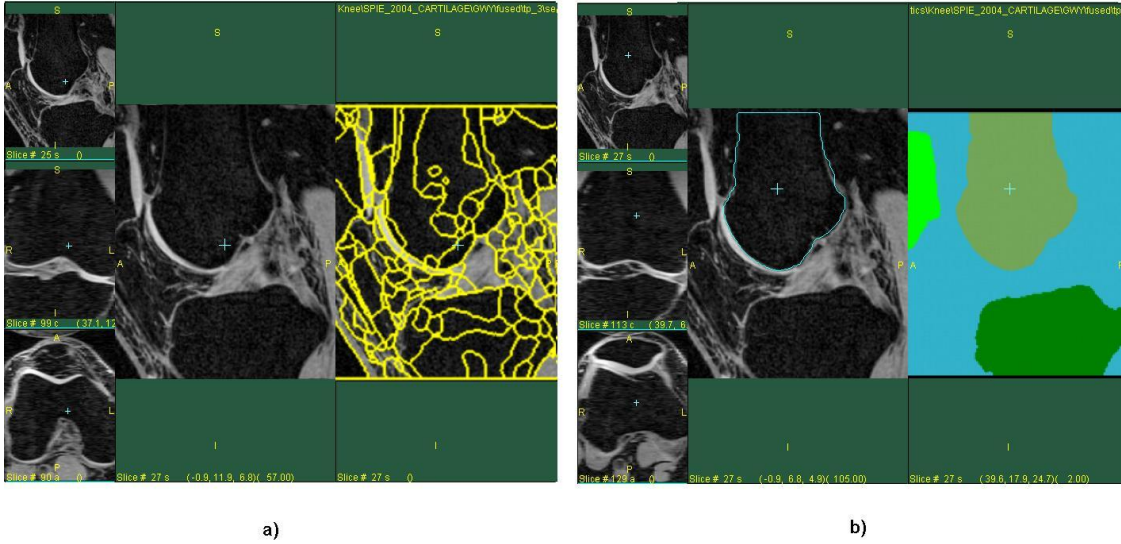


Figure 3. Bone extraction. Left the input segmentation from the unsupervised algorithm. Right, the labeled segmentation. The user identifies the femur, the patella and the tibia, the rest of the tissues are automatically excluded.

image space. Once the segmentation map is mapped into the original space this segmentation is then relaxed to match the signal properties of the original image using the Gibbs model suggested by Geman¹⁶ and an Iterated Conditional Mode optimization.¹⁸ After the relaxation the user observes the segmentation and starts merging all the regions that belong to the bone tissue. The merging process is very fast and the users typically requires less than five minutes to merge all the regions of the femur tibia and patella. Figure 3 shows the results of the unsupervised segmentation and the results after the bones have been labeled as femur tibia and patella.

2.2.2. Cartilage Extraction

After the bone labeling process, the cartilage extraction is done by first extracting the cartilage-bone interface. This interface is found by searching all the bone surface points at a given direction and selecting the neighbors surface points that are hyper-intense compared to the mean and standard deviation of the values of the neighbor points. The given direction is defined as the one where the cartilage lies with respect to the bone. i.e, the tibia cartilage lies superior to the bone, the patella cartilage lies posterior to the bone and the femur cartilage is anterior, posterior and inferior to the femur. Figure 4a) shows the cartilage extraction dialog where the software ask the user for the bone labels and the cartilage orientations. The neighbors points n that are hyper-intense $f(n) > \mu + t_s \sigma$; where μ is the mean value of the signal intensity and σ is the standard deviation of the signal intensity, and whose normal, $\mathbf{N}(n)$, is along the cartilage orientation, \mathbf{d} , $\mathbf{N}(n) \cdot \mathbf{d} < t_d$ are labeled as possible cartilage points. t_s and t_d are the threshold values that define if the points are hyper-intense or whose normals are in the cartilage direction. Furthermore, using some knowledge of the knee anatomy we find the orientation of the femur and the location of the femoral notch using the approach described in Tamez.¹¹ This knowledge is used to remove all the misclassified surface points from the femoral notch and tibia spine surfaces.

After the neighboring point classification, subject specific deformable models for the tibia, femur and patella are automatically built from these points by dilating the neighboring points in direction of the bones surface normals by the amount specified by the user. The dilatation uses a 3D competitive region growing algorithm. The 3D competitive region growing algorithm dilates all the surface points from the three cartilage models that share a background neighbor. Once the neighbor label changed to any other cartilage label or bone label the dilatation of that point is stopped as seen in Figure 5a). The dilated points now are surface render using the surface reconstruction algorithm used at Pakin.¹⁴ The femoral surface can be seen in figure 5b) where each

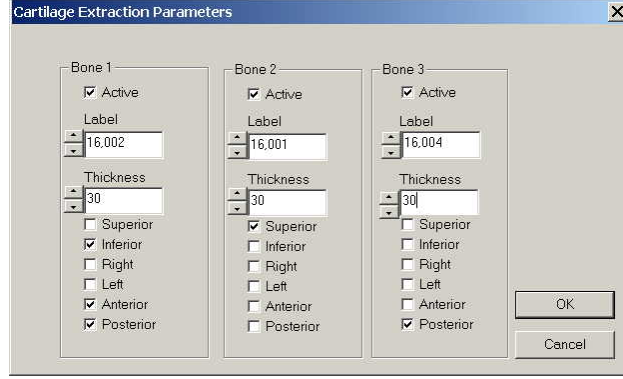


Figure 4. Cartilage Extraction dialog. The user inputs the bone labels, the cartilage location in the bone and the expected cartilage thickness

node of the surface now is a member of the deformable model. The dynamics of the deformable model will be governed by a spring-mesh model with curvature constraints whose external energy is derived by the image content. Each node of the model will follow the trajectory defined by the differential equation:

$$m \frac{\partial^2 \mathbf{x}}{\partial t^2} = f_{int}(\mathbf{x}) + f_{ext}(\mathbf{x}) - \nu \frac{\partial \mathbf{x}}{\partial t}; \quad (1)$$

where \mathbf{x} is the current node location, m is the mass of the node, f_{int} is the total internal force, and f_{ext} is the total external force. The internal force is derived by the spring interaction of each node to its neighbors in a damping media. The external force is derived from the first band of the image data $f(\mathbf{x})$. Under the assumption that the cartilage is an hyper-intense tissue next to the bone tissue, and that the external force acts parallel to the node dilatation trajectory, $\mathbf{n}_d(\mathbf{x})$, the equation:

$$f_{ext}(\mathbf{x}) = \mathbf{n}_d(\mathbf{x}) \cdot \begin{cases} a & \text{if } |f(\mathbf{x}) - \max_d| < c\sigma(\mathbf{x}) \\ -b & \text{otherwise} \end{cases} \quad (2)$$

will drive the deformable surface to the external cartilage boundary; where \max_d is the maximum intensity along the predicted node trajectory, $\sigma(\mathbf{x})$ is the local standard deviation of the intensity values along the deformable surface, and a, b, c are constants that will define the stability of the system. In other words, at each node the deformable surface will feel a contracting force parallel to the surface normal until it reaches a point that is similar to the maximum intensity observed in direction of the propagation front. The solution of this equation will minimize the total energy of the system; which will deform the surface of the model to the external cartilage layer.

Once the deformable system reaches an equilibrium the next step, if necessary, is the correction of the cartilage boundaries found by the deformable model. The major source of errors are in points where the deformable model identifies possible cartilage tissue; when in reality it was muscle or other soft tissue adjacent to the bone. These errors have to be corrected by the analyst. For that purpose we developed a system that uses two major tools: A region eraser and a contour editor. The region eraser allows the user to erase all the classified voxels inside a region of interest (ROI) defined by the user using a free-hand ROI. The second tool allows the user to adjust the contour of the classified tissues to the user specified location. Once the user removes all the misclassified voxels and corrects the contour boundaries the next step is the relaxation of the region boundaries. For that purpose we use a Gibbs random field of the classification-image data pair.¹⁶ The Gibbs model allows the relaxation of the classification via the maximization of the a-posteriori probability. The maximization algorithm used for the relaxation is the iterated conditional mode (ICM) algorithm, that gives very good results for systems that are close to the correct solution. After the relaxation the user has the freedom to correct any boundary errors if he chose. However, after this stage we can proceed to the extraction of the cartilage morphometry. Figure 6 shows the 3D reconstruction of the cartilage and bone.

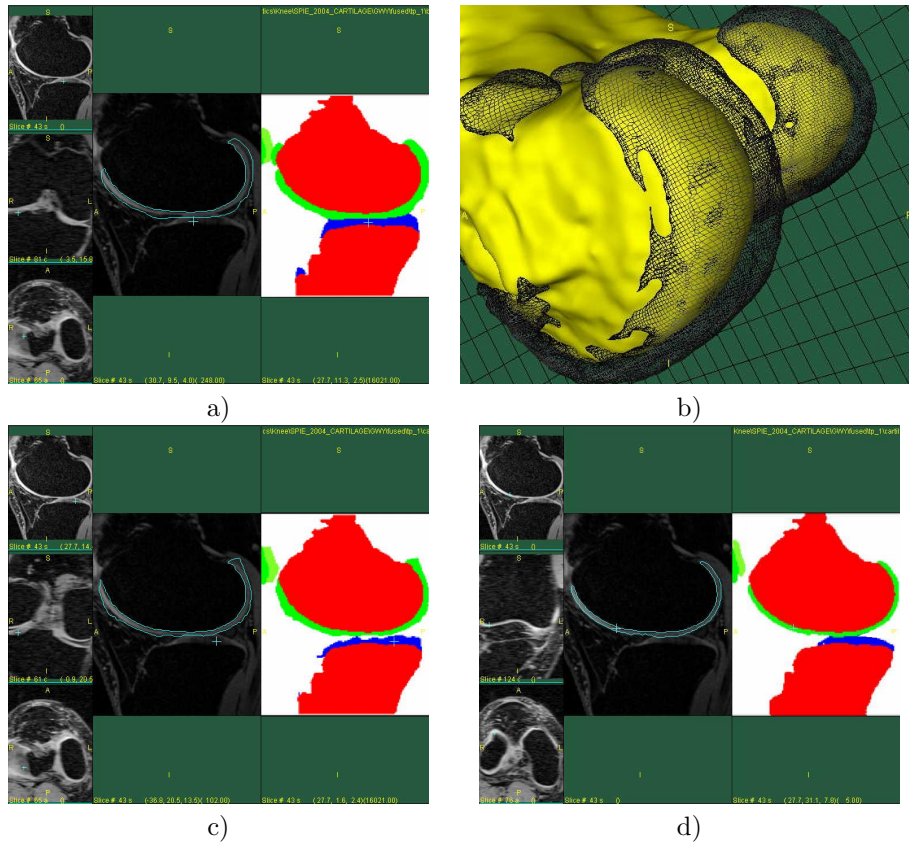


Figure 5. Cartilage Extraction process. a) a single slice trough the deformable model. b) a 3D reconstruction of the model overlaid the 3D reconstruction of the femur. c) the deformable model after equilibrium. d) Final bone-cartilage segmentation.

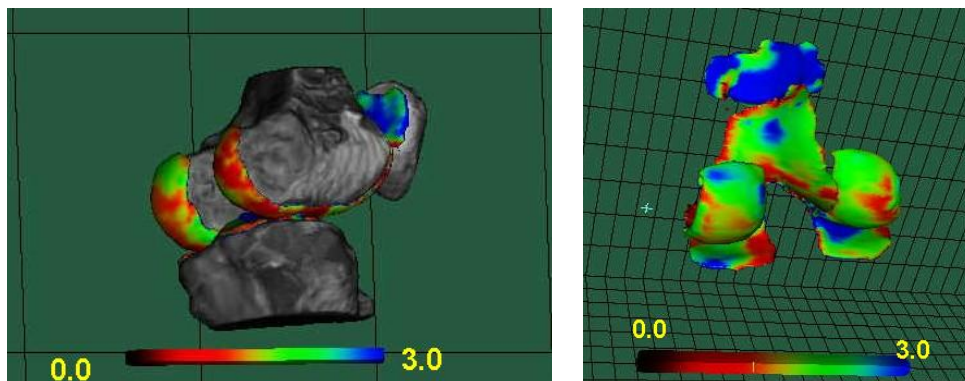


Figure 6. 3D reconstructions of the bones and the cartilage. The color map represent different cartilage thickness.

2.2.3. Morphometry: Volume, Surface, Thickness and Contact Analysis

The volume, surface area, thickness, and contact analysis are extracted from the the reconstructed surface of the classified cartilage tissue. The surface extraction is done using the method described in Pakin.¹⁴ This surface extraction method has the ability to adjust the surface boundaries according to the partial volume information estimation at each voxel. This is a very nice feature that allows continuous and more reproducible metrics. The extracted surface is a polygon defined by thousands of triangular patches. The volume is computed by the continuous integration of the polygonal surface, the area is computed via the integration of all the triangular patches on the surface, and the cartilage-bone contact area is also the integration of the surface that is in contact to the bone tissue.

The thickness computation is carried out by computing at each node the distance of one surface to the opposite surface. The opposite surface is defined by the first interested triangular surface patch intersected by the line defined by the normal at the point. The cartilage thickness computed by using this method is a continuous variable unlike the discrete nature of most current methods^{19, 4}

3. RESULTS

Two major experiments were done with the long term scan volunteer data. The five scans were divided into two groups of tree scans. One group contained three scans of fat suppress data and the other group was composed by tree scans with dual pulse sequences: a fat suppress GRE and a T_2 GRE data. All The data was segmented using the approach described in the paper. The fused data was segmented twice to asses re-segmentation variation. Therefore, a set of 9 analysis were done on the first volunteer. The user took in average 5 minutes to do the bone segmentation on the fused data sets. On the other hand, it took more than 20 minutes for the segmentation of the fat suppressed images. The mayor problem was that the segmentation algorithm didn't have enough information to separate the bone tissue from the surrounding fatty tissue and the background. That fact made the bone extraction harder and the user had to do a lot of editing before having a complete bone segmentation. Table 1 summarizes the measurements done on the first group of experiments. The data shows that the femur segmentation is highly reproducible; while the segmentation of the medial cartilage is the cartilage regions where more variation was measured. No statistical difference was observed between the segmentation of the fat suppressed images and the segmentation using the fused-data sets. The main difference was in the time. The average user took 20 minutes to do the bone segmentation from the fat suppressed images while it only took, on average, seven minutes to get the bones extracted from the fused data sets. This shows the greater advantage of the fused set. The re-segmentation experiment the user was asked to re-segment the fused data set two days after the original segmentation. Table 2 summarizes the results the observed coefficient of variations (C.V.) are very similar to the ones gotten using the scan-rescan data. The correlation between the observed thickness are plotted in figure 7. The correlation was very high $R^2 = 0.97$. To get an idea of the amount of work per surface area, the same figure plots the correlation of the expected thickness after dividing the volume over the average observed surface area. This plot shows also a very high correlation between segmentations ($R^2 = 0.93$). The average C.V. for the whole knee is presented in table 3. This table shows that the whole knee analysis resulted on an average C.V. of 2.6% for all the measurements. Segmentations were also done to OA subjects; but scan-rescan data was not available at the time of the publication. The segmentation experience of these data sets was positive; taking a little more time for the user to do the cartilage segmentation around 40 minutes; but not far from the average 30 minutes from healthy volunteers.

4. DISCUSSION

This paper proposes a method that offers a systematic approach for the bone-cartilage analysis of knee joints. It offers the ability to extract the tibia, the femur, and the patella. It also extracts the femoral cartilage, the tibia medial and lateral cartilage and the patella cartilage. The entire analysis can be done in less than 40 minutes by trained observers without compromising the quality of the analysis. The method employs the latest development on multi-spectral cartilage segmentation, 3D deformable templates, stochastic relaxation and accurate surface reconstruction. Preliminary results show that our system compares well with all the other published methods and it offers the ability that extracting more information can be achieved without much more analyst time. Meta

Volumes		Femur	Whole Tibia	Patella	Tibia Medial	Tibia Lateral
Fat Suppressed	Mean	7843.29	3402.75	2700.28	1506.14	1893.74
	Std Dev	59.89	90.65	38.84	1.61	92.75
	C.V.	0.8%	2.7%	1.4%	0.1%	4.9%
Fused	Mean	7644.03	3371.59	2647.21	1468.06	1903.50
	std dev	110.31	195.24	88.28	145.68	71.52
	C.V.	1.4%	5.8%	3.3%	9.9%	3.8%
Surface Area		Femur	Whole Tibia	Patella	Tibia Medial	Tibia Lateral
Fat Suppressed	Mean	8565.91	3220.40	1992.88	1612.99	1607.44
	Std Dev	152.20	141.29	74.99	113.00	33.77
	C.V.	1.8%	4.4%	3.8%	7.0%	2.1%
Fused	Mean	8460.91	3244.04	1963.51	1613.47	1630.29
	std dev	165.42	123.38	24.98	170.53	48.88
	C.V.	2.0%	3.8%	1.3%	10.6%	3.0%
Contact Area		Femur	Whole Tibia	Patella	Tibia Medial	Tibia Lateral
Fat Suppressed	Mean	3720.84	1414.48	854.33	742.92	712.73
	Std Dev	82.95	38.12	28.74	49.52	14.58
	C.V.	2.2%	2.7%	3.4%	6.7%	2.0%
Fused	Mean	3660.61	1469.67	856.62	744.71	724.87
	std dev	126.04	63.46	3.06	83.58	23.21
	C.V.	3.4%	4.3%	0.4%	11.2%	3.2%
Thickness		Femur	Whole Tibia	Patella	Tibia Medial	Tibia Lateral
Fat Suppressed	Mean	1.82	2.24	3.00	1.94	2.62
	Std Dev	0.02	0.18	0.09	0.17	0.17
	C.V.	0.8%	8.2%	2.9%	8.5%	6.6%
Fused	Mean	1.79	2.17	3.00	1.84	2.58
	std dev	0.02	0.08	0.08	0.05	0.18
	C.V.	1.3%	3.5%	2.6%	2.8%	7.1%

Table 1. Scan-Rescan of a female volunteer

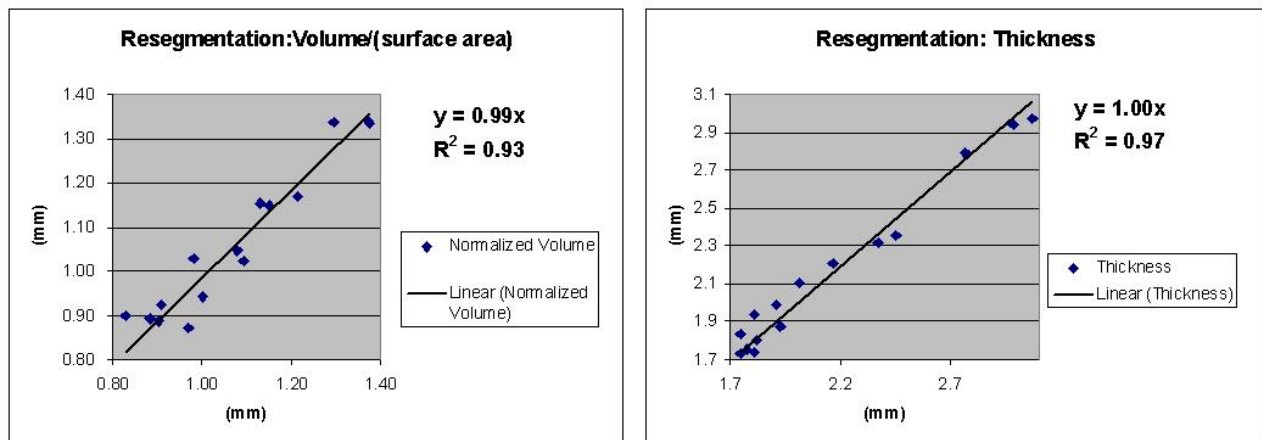


Figure 7. Correlation plots of the re-segmentation analysis of the estimated thickness (volume over surface area) and the true observed thickness

		Femur	Whole Tibia	Patella	Tibia Medial	Tibia Lateral
Volume	Mean	7,654.57	3,340.72	2,635.24	1,444.29	1,895.96
	SDD	126.60	192.22	86.95	138.37	57.06
	C.V.	1.2%	4.1%	2.3%	6.8%	2.1%
		Femur	Whole Tibia	Patella	Tibia Medial	Tibia Lateral
Surface Area	Mean	8,500.74	3,204.84	1,962.67	1,571.75	1,632.66
	SDD	138.24	176.91	56.78	163.29	43.79
	C.V.	1.1%	3.9%	2.0%	7.3%	1.9%
		Femur	Whole Tibia	Patella	Tibia Medial	Tibia Lateral
Contact Area	Mean	3,670.01	1,448.89	850.80	721.60	727.16
	SDD	117.82	69.14	7.22	62.29	18.31
	C.V.	2.3%	3.4%	0.6%	6.1%	1.8%
		Femur	Whole Tibia	Patella	Tibia Medial	Tibia Lateral
Thickness	Mean	1.79	2.19	3.00	1.87	2.57
	SDD	0.01	0.07	0.01	0.08	0.12
	C.V.	0.2%	2.3%	0.1%	3.2%	3.2%
		Femur	Whole Tibia	Patella	Tibia Medial	Tibia Lateral
V/S	Mean	0.90	1.04	1.34	0.92	1.16
	SDD	0.01	0.06	0.04	0.09	0.03
	C.V.	1.2%	4.1%	2.3%	6.8%	2.1%

Table 2. Re-segmentation analysis of the female volunteer

	Mean	SDD	C.V.
Volume	3,394.155	112.795	2.3%
Surface Area	3,374.530	125.101	2.6%
Contact Area	1,483.690	62.972	3.0%
Thickness	2.283	0.066	2.1%
V/S	1.073	0.047	3.1%

Table 3. Average CV form the whole knee analysis

analysis can be done to extract the subchondral bone plate, the 3D joint space analysis^{11,20} the bone marrow after the registration of spin-echo sequences, etc. All these advantages are not present on all other methods that only extract cartilage tissue. Although the automated cartilage analysis presented in this paper is still far from being an unsupervised method for the knee cartilage extraction, it offers a scalable alternative for the analysis of hundreds of data sets. The modular approach allows the use of multiple human image-processors for a single cartilage extraction. A novice user can be trained for the bone labeling step, an experienced user can be used to extract the cartilage, and a radiologist qualified user can be responsible of the quality assurance of the final product after the relaxation step. The amount of time involved at each step is less than half an hour which is reasonable to avoid user fatigue. The other advantage of the proposed scheme is that the deformable model can be improved by the development of an accurate knee atlas.²¹ Therefore, in the future the cartilage editing step can be completely avoided and just leaving the expert quality assurance for the final product review. The perfect deformable model derived from the human knee atlas is not far from being a reality. Right now, there are several studies around the world that are acquiring hundreds of MRI data sets of the human knee; their analysis will yield an accurate knee atlas that can easily be incorporated into our system.

ACKNOWLEDGMENTS

The authors would like to thank Gwy Suk and Larry Molinelli for their efforts related to this work. Financial support was provided by the Department of Radiology of the University of Rochester Medical Center and VirtualScopics, L.L.C.

REFERENCES

1. F. Eckstein and K. H. Englmeier, "Quantitative image analysis: software systems in drug development trials," *DRUG DISCOVERY TODAY* **8**(20), pp. 922–923, 2003.
2. C. A. McGibbon, J. B. E. Yeh, and W. E. Palmer, "Accuracy of cartilage and subchondral bone spatial thickness distribution from mri," *JOURNAL OF MAGNETIC RESONANCE IMAGING* **17**(6), pp. 703–715, 2003.
3. C. A. McGibbon, "Inter-rater and intra-rater reliability of subchondral bone and cartilage thickness measurement from mri," *MAGNETIC RESONANCE IMAGING* .
4. C. Glaser, R. Burgkart, A. Kutschera, K. H. Englmeier, M. Reiser, and F. Eckstein, "Femoro-tibial cartilage metrics from coronal mr image data: Technique, test-retest reproducibility, and findings in osteoarthritis," *MAGNETIC RESONANCE IN MEDICINE* **50**(6), pp. 1229–1236, 2003.
5. C. Kauffmann, P. Gravel, B. Godbout, A. Gravel, G. Beaudoin, J. Raynauld, J. Martel-Pelletier, J. Pelletier, and J. A. de Guise, "Computer-aided, method for quantification of cartilage thickness and volume changes using mri: Validation study using a synthetic model," *IEEE TRANSACTIONS ON BIOMEDICAL ENGINEERING* **50**(8), pp. 978–988, 2003.
6. J. Raynauld, C. Kauffmann, G. Beaudoin, M. Berthiaume, J. A. de Guise, D. A. Bloch, F. Camacho, B. Godbout, R. Altman, M. Hochberg, J. M. Meyer, G. Cline, J. P. Pelletier, and J. Martel-Pelletier, "Reliability of a quantification imaging system using magnetic resonance images to measure cartilage thickness and volume in human normal and osteoarthritic knees," *OSTEOARTHRITIS AND CARTILAGE* **11**(5), pp. 351–360, 2003.
7. F. Eckstein, L. Heudorfer, S. Faber, R. Burgkart, K. Englmeier, and M. Reiser, "Long-term and resegmentation precision of quantitative cartilage mr imaging (qmri)," *OSTEOARTHRITIS AND CARTILAGE* **10**(12), pp. 922–928, 2002.
8. A. Mohr, "The value of water-excitation 3d flash and fat-saturated pdw tse mr imaging for detecting and grading articular cartilage lesions of the knee," *SKELETAL RADIOLOGY* **32**(7), pp. 396–402, 2003.
9. H. Yoshioka, M. Alley, D. Steines, K. Stevens, E. Rubesova, M. Genovese, M. Dillingham, and P. Lang, "Imaging of the articular cartilage in osteoarthritis of the knee joint: 3d spatial-spectral spoiled gradient-echo vs. fat-suppressed 3d spoiled gradient-echo mr imaging," *JOURNAL OF MAGNETIC RESONANCE IMAGING* **18**(1), pp. 66–71, 2003.

10. C. A. McGibbon, J. Bencardino, and W. E. Palmer, "Subchondral bone and cartilage thickness from mri: effects of chemical-shift artifact," *MAGNETIC RESONANCE MATERIALS IN PHYSICS BIOLOGY AND MEDICINE* **16**(1), pp. 1–9, 2003.
11. J. G. Tamez-Pena, L. Lerner, J. Yao, A. D. Salo, and S. M. S. Totterman, "Evaluation of distance maps from fast gre mri as a tool to study the knee joint space," *SPIE: Medical Imaging: Physiology and Function: Methods, Systems, and Applications* **5031**, pp. 551–562, 2003.
12. J. G. Tamez-Pena, S. Totterman, and K. Parker, "Unsupervised statistical segmentation of multispectral volumetric mri images," in *Medical Imaging: Image Processing, Proceedings of the SPIE* **3661**, pp. 300–311, 1999.
13. J. Tamez-Pena, S. Totterman, and K. Parker, "The integration of automatic segmentation and motion tracking for 4d reconstruction and visualization of musculoskeletal structures," *IEEE Workshop on Biomedical Image Analysis*, pp. 154–163, 1998.
14. S. K. Pakin, J. G. Tamez-Pena, S. Totterman, and K. Parker, "Segmentation, surface extraction, and thickness computation of articular cartilage," in *Medical Imaging: Image Processing, Proc. SPIE* **4684**, pp. 155–166, 2002.
15. T. Stammberger, F. Eckstein, M. Michaelis, K. Englmeier, and M. Reiser, "Interobserver reproducibility of quantitative cartilage measurements: Comparison of b-spline snakes and manual segmentation," *MAGNETIC RESONANCE IMAGING* **17**(7), pp. 1033–1042, 1999.
16. S. Geman and D. Geman, "Stochastic relaxation, gibbs distribution, and bayesian restoration of images," *IEEE Trans. Patt Anal. Mach. Intel* **6**, pp. 721–741, 1984.
17. J. Maintz and M. Viergever, "A survey of medical image registration," *Medical Image Analysis* **2**, pp. 1–37, 1998.
18. T. N. Pappas, "An adaptive clustering algorithm for image segmentation," *IEEE Trans. Signal Proc.* **SP-40**, pp. 901–914, 1992.
19. F. Eckstein, J. Westhoff, H. Sittek, K. Maag, M. Haubner, S. Faber, K. Englmeier, and M. Reiser, "In vivo reproducibility of three-dimensional cartilage volume and thickness measurements with mr imaging," *AMERICAN JOURNAL OF ROENTGENOLOGY* **170**(3), pp. 593–597, 1998.
20. S. Martelli and V. Pinskerova, "The shapes of the tibial and femoral articular surfaces in relation to tibiofemoral movement," *Journal of Bone and Joint Surgery* **84B**(4), pp. 607–613, 2002.
21. E. J. Alexander and T. P. Andriacchi, "A model based approach for efficient segmentation of knee cartilage from mr image data," *ASME Bioeng Div Publ BED* **51**, pp. 105–106, 2001.